Fuel 197 (2017) 290–297

Contents lists available at ScienceDirect

Fuel

journal homepage: www.elsevier.com/locate/fuel

Full Length Article

Numerical simulations on the effect of potassium on the biomass fast pyrolysis in fluidized bed reactor

Qitai Eri [a], Xinjun Zhao [a], Panneerselvam Ranganathan [b], Sai Gu [c,*]

[a] School of Energy and Power Engineering, Beihang University, PR China
[b] Environmental Technology Division, CSIR-National Institute for Interdisciplinary Science and Technology, Trivandrum, India
[c] Department of Chemical and Process Engineering, University of Surrey, UK

HIGHLIGHTS

- CFD model developed for fast pyrolysis of cellulose with potassium.
- Effect of potassium on the products yield and composition has been studied and analyzed.
- Effect of reactor temperature has been analyzed.
- Effect of unstable flow on the products yield has been studied.

ARTICLE INFO

Article history:
Received 25 February 2016
Received in revised form 9 January 2017
Accepted 31 January 2017
Available online 23 February 2017

Keywords:
Biomass fast pyrolysis
Potassium
Fluidized bed
Multi-fluid model

ABSTRACT

In this study, the effect of potassium on the cellulose fast pyrolysis in a fluidized bed reactor has been studied using Computational Fluid Dynamics (CFD). A multiphase pyrolysis model of cellulose has been implemented by integrating the hydrodynamics of the fluidized bed with an adjusted cellulose pyrolysis mechanism that accounts for the effect of potassium. The model has been validated with the reported experimental data. The simulation results show that potassium concentration and reactor temperature have a significant effect on the yield and component of cellulose pyrolysis products. The product yields fluctuate is caused by the unstable flow in the fluidized bed. The result shows that the increased potassium concentration in the cellulose causes a significant increase of the gas and char yields and reduction in the bio-oil. Also, the dramatic composition variations in bio-oil and gas were observed due to the inhibition of fragmentation, and the depolymerization reaction of activated cellulose, and the catalysis of the depolymerization reaction of cellulose. It is also found that the increase in reactor temperature greatly enhances the endothermic pyrolysis reaction, which leads to the significant changes in the yield and composition of cellulose pyrolysis products.

1. Introduction

Fast pyrolysis is one of the most promising technologies for producing bio-oil, gas and char from biomass [1–3]. Fluidized bed reactor is widely used in biomass fast pyrolysis, as they have good temperature control and high heat transfer rates [3,4]. The thermochemical conversion of biomass in fluidized beds has been extensively investigated using both experimental and numerical methods in the literature [5–8].

Biomass usually contains considerable amounts of alkali and alkaline earth metallic species (AAEMs) such as sodium, potassium, calcium, etc. Many studies have reported that AAEMs play an important role in biomass pyrolysis reactions [9–15]. Shimada et al. [9] studied the effect of AAEMs on cellulose pyrolysis and found that potassium chloride and sodium chloride caused a reduced levoglucosan yield and increased the yield of water, carbon monoxide, and char. Patwardhan et al. [10] found that potassium chloride and sodium chloride led to a significant increase in the yield of low molecular weight species, while there was a severe reduction of the levoglucosan yield. Rutkowski [11] investigated the effects of potassium carbonate on cellulose pyrolysis. The results indicate that potassium carbonate influenced the decomposition temperature of cellulose and the composition of a pyrolysis product significantly. Hu et al. [12] investigated the effects of the inherent AAEMs on biomass pyrolysis. The results indicate that inherent AAEMs can enhance the production of carbon dioxide

* Corresponding author.
E-mail address: sai.gu@surrey.ac.uk (S. Gu).

http://dx.doi.org/10.1016/j.fuel.2017.01.109
0016-2361/

and hydrogen, and the decomposition of levoglucosan significantly.

Computational Fluid Dynamics (CFD) has been widely used for modeling of the hydrodynamics, heat transfer and chemical reactions inside the fluidized bed, and various CFD models for biomass pyrolysis process in fluidized bed have been developed that can be categorized into Euler–Lagrangian and Euler–Euler models. The Euler–Euler model could simulate the biomass pyrolysis in a fluidized bed reactor effectively. It includes the space-time evolution of pyrolysis products in a fluidized bed, the interaction between the sand, biomass and gases, and the effects of operating conditions on the yield and composition of pyrolysis products [16–23]. The Euler-Lagrangian model could simulate the pyrolysis of discrete biomass particle in a fluidized bed reactor accurately, but it needs huge computational cost [24–27].

There are several experimental studies on the effect of potassium on the cellulose fast pyrolysis. However, a numerical study has not been conducted and published so far. In this work, a model of cellulose fast pyrolysis in a fluidized bed based on the Eulerian multiphase flow framework has been developed. The spatial-temporal evolutions of products from cellulose fast pyrolysis in a fluidized bed are studied using CFD. The effects of potassium concentration and reactor temperature on the composition and yield of cellulose fast pyrolysis products are intensively investigated.

2. Model description

The sketch of the numerically simulated 300 g/h fluidized bed reactor of Aston University is shown in Fig. 1, and the specifications of the computational domain can be seen in Table 1 [28]. 2-D simulations are performed in the present work. The fluidization gas is preheated pure nitrogen, which flows from the bottom of the reactor at a velocity of 0.744 m/s. The biomass is injected from the beginning of the simulation at the side of the reactor. A constant biomass particle diameter of 0.6 mm is used in all simulations. The initial biomass is cellulose with potassium concentration varied from 0.0 wt.% to 1.0 wt.%.

3. Computational model

In order to accurately simulate the biomass pyrolysis in a fluidized bed reactor, the gas-solid flows are modeled using an Euler–Euler multiphase model, and the cellulose pyrolysis reactions are simulated using a detailed chemical kinetic model. These models were solved using the CFD software ANSYS Fluent 15.0.

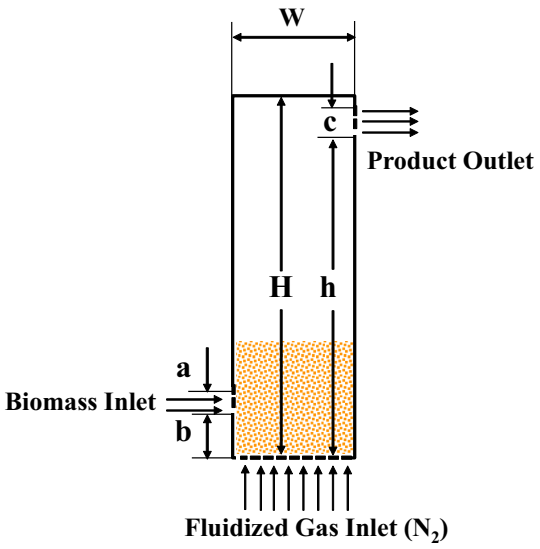

Fig. 1. Schematic diagram of the 2-D fluidized bed reactor.

Table 1
Specifications of the computational domain [28].

Reactor height, H	257 mm	Reactor width, W	41 mm
Biomass inlet diameter, a	14 mm	Biomass inlet height, b	16 mm
Product outlet diameter, c	7 mm	Product outlet height, h	244 mm

3.1. Multiphase flow governing equations

There are three phases in the fluidized bed reactor, i.e., gas phase, biomass particles and sand. The gas phase includes nitrogen as a fluidization gas and gas products from biomass fast pyrolysis. The biomass particle includes unreacted cellulose, activated cellulose which is an intermediate product of cellulose pyrolysis and char produced from biomass pyrolysis. In the Euler–Euler multiphase model, all the three phases are treated as interpenetrating continua. The gas phase is the primary phase and the solid phases, i.e., biomass particles and sand, are considered as secondary phases.

3.1.1. Gas phase

The continuity equation for the gas phase is

$$\frac{\partial}{\partial t}(\alpha_g \rho_g) + \nabla \cdot (\alpha_g \rho_g \vec{v}_g) = \dot{m}_g \tag{1}$$

where $\vec{v}_g$ and ρ_g are the velocity and density of gas, respectively, $\dot{m}_g$ is the mass transfer between phases and α_g is the gas volume fraction [29].

The species transport equation is

$$\frac{\partial}{\partial t}(\alpha_g \rho_g Y_k) + \nabla \cdot (\alpha_g \rho_g \vec{v}_g Y_k) = \sum_{m=1}^{M} \dot{m}_{s_m,gk} \tag{2}$$

where Y_k is the mass fraction of kth species, $\dot{m}_{s_m,gk}$ is the net mass exchange between the gas phase component k and the solid phase m, and M is the total number of solid phases [29].

The conservation of momentum for the gas phase is

$$\frac{\partial}{\partial t}(\alpha_g \rho_g \vec{v}_g) + \nabla \cdot (\alpha_g \rho_g \vec{v}_g \vec{v}_g) = -\alpha_g \nabla p + \alpha_g \rho_g \vec{g} + \nabla \cdot \bar{\bar{\tau}}_g + \sum_{m=1}^{M} (K_{s_m g}(\vec{v}_{s_m} - \vec{v}_g) + \dot{m}_{s_m g} \vec{v}_{s_m}) \tag{3}$$

where p is the pressure, $\vec{g}$ is the acceleration of gravity, $\bar{\bar{\tau}}_g$ is the gas phase stress-strain tensor, and $K_{s_m g}$ is the interphase momentum exchange coefficient between mth solid phase and gas phase.

Gas-solid exchange coefficient is given by Gidaspow [30]. Although Gidaspow drag model does not work well in the freeboard region of fluidized bed reactor, according to the previous studies reported in the literature [8,18], this model is suitable for simulating the biomass pyrolysis in the bubbling fluidized bed. The model equations are

when $\alpha_g > 0.8$, the exchange coefficient K_{sg} is

$$K_{sg} = \frac{3}{4} C_D \frac{\alpha_s \alpha_g \rho_g |\vec{v}_s - \vec{v}_g|}{d_s} \alpha_g^{-2.65} \tag{4}$$

where

$$C_D = \frac{24}{\alpha_l Re_s}\left[1 + 0.15(\alpha_g Re_s)^{0.687}\right] \tag{5}$$

when $\alpha_g \leqslant 0.8$,

$$K_{sg} = 150\frac{\alpha_s(1-\alpha_g)\mu_g}{\alpha_g d_s^2} + 1.75\frac{\rho_g \alpha_s |\vec{v}_s - \vec{v}_g|}{d_s} \quad (6)$$

The energy conservation equation for gas phase is

$$\frac{\partial}{\partial t}(\alpha_g \rho_g h_g) + \nabla \cdot (\alpha_g \rho_g \vec{u}_g h_g) = \alpha_g \frac{\partial p}{\partial t} + \bar{\bar{\tau}}_g : \nabla \vec{v}_g - \nabla \cdot \vec{q}_g + \Delta H_g + \sum_{m=1}^{M} h_{gs_m} a_{gs_m}(T_g - T_s) \quad (7)$$

where $\vec{q}_g$ is the heat flux, ΔH_g is the heat of the chemical reaction in the gas phase, and h_{gs_m} is the volumetric heat exchange between the gas phase and mth solid phase which is given by Gunn [31]

$$h_{gs} = \frac{6k_g \alpha_g \alpha_s Nu_s}{d_s^2} \quad (8)$$

$$Nu_s = (7 - 10\alpha_g + 5\alpha_g^2)(1 + 0.7Re_s^{0.2}Pr^{1/3}) + (1.33 - 2.4\alpha_g + 1.2\alpha_g^2)Re_s^{0.7}Pr^{1/3} \quad (9)$$

The gas phase stress-strain tensor $\bar{\bar{\tau}}_g$ in Eqs. (3) and (7) is defined as

$$\bar{\bar{\tau}}_g = \alpha_g \mu_g (\nabla \vec{v}_g + \nabla \vec{v}_g^T) + \alpha_g \left(\lambda_g - \frac{2}{3}\mu_g\right) \nabla \cdot \vec{v}_g \bar{\bar{I}} \quad (10)$$

where μ_g denotes the molecular viscosity of gas phase, while λ_g denotes the bulk viscosity of gas phase.

3.1.2. Solid phase

The continuity equation for solid phase m is

$$\frac{\partial}{\partial t}(\alpha_{s_m} \rho_{s_m}) + \nabla \cdot (\alpha_{s_m} \rho_{s_m} \vec{v}_{s_m}) = \dot{m}_{s_m} \quad (11)$$

where $\vec{v}_{s_m}$ is the velocity of solid phase m, and $\dot{m}_{s_m}$ is the mass transfer from the mth solid phase to gas phase.

The conservation of momentum for the mth solid phase is

$$\frac{\partial}{\partial t}(\alpha_{s_m} \rho_{s_m} \vec{v}_{s_m}) + \nabla \cdot (\alpha_{s_m} \rho_{s_m} \vec{v}_{s_m} \vec{v}_{s_m}) = -\alpha_g \nabla p + \alpha_{s_m} \rho_{s_m} \vec{g} + \nabla \cdot \bar{\bar{\tau}}_{s_m} + \sum_{n=1}^{N} \left(K_{ns_m}(\vec{v}_n - \vec{v}_{s_m})\right) \quad (12)$$

where K_{ns_m} is the momentum exchange coefficient between sth and nth gas phase or solid phase.

The energy conservation equation for solid phase m is

$$\frac{\partial}{\partial t}(\alpha_{s_m} \rho_{s_m} h_{s_m}) + \nabla \cdot (\alpha_{s_m} \rho_{s_m} \vec{u}_{s_m} h_{s_m}) = \alpha_{s_m} \frac{\partial p_{s_m}}{\partial t} + \bar{\bar{\tau}}_{s_m} \cdot \nabla \vec{u}_{s_m} - \nabla \cdot \vec{q}_{s_m} + \Delta H_{s_m} + h_{s_m g} a_{s_m g}(T_{s_m} - T_g) \quad (13)$$

where $\vec{q}_{s_m}$ is the heat flux; ΔH_{s_m} is the heat of reaction in the mth solid phase [29].

The solid phase stress-strain tensor $\bar{\bar{\tau}}_{s_m}$ in Eqs. (12) and (13) is defined as

$$\bar{\bar{\tau}}_{s_m} = -P_{s_m}\bar{\bar{I}} + \alpha_{s_m}\mu_{s_m}(\nabla \vec{v}_{s_m} + \nabla \vec{v}_{s_m}^T) + \alpha_{s_m}\left(\lambda_{s_m} - \frac{2}{3}\mu_{s_m}\right)\nabla \cdot \vec{v}_{s_m}\bar{\bar{I}} \quad (14)$$

where μ_{s_m} denotes the solid shear viscosity of solid phase which is given by (15), while λ_{s_m} denotes bulk viscosity of solid phase which is given by (16) and P_{s_m} is the solid phase pressure given by (17).

$$\mu_{s_m} = \mu_{s_m,col} + \mu_{s_m,kin} + \mu_{s_m,fr} \quad (15)$$

where $\mu_{s_m,col}$, $\mu_{s_m,kin}$, and $\mu_{s_m,fr}$ are the collisional viscosity, the kinetic viscosity, and the frictional viscosity, respectively.

$$\lambda_{s_m} = \frac{4}{3}\alpha_{s_m}\rho_{s_m}d_{s_m}g_{0,s_m s_m}(1 + e_{s_m s_m})\left(\frac{\theta_{s_m}}{\pi}\right)^{1/2} \quad (16)$$

where $e_{s_m s_m}$ is the coefficient of restitution for particle collisions, $g_{0,s_m s_m}$ is the radial distribution function, and θ_{s_m} is the granular temperature.

$$P_{s_m} = \alpha_{s_m}\rho_{s_m}\theta_{s_m} + 2\rho_{s_m}(1 + e_{s_m s_m})\alpha_{s_m}^2 g_{0,s_m s_m}\theta_{s_m} \quad (17)$$

The granular temperature for the mth solids phase θ_{s_m} is proportional to the kinetic energy of the particles random motion. The formal expression is

$$\theta_{s_m} = \frac{1}{3}u_{s_m,i}u_{s_m,i} \quad (18)$$

where $u_{s_m,i}$ represents the ith component of the fluctuating solids velocity.

The transport equation derived from kinetic theory is

$$\frac{3}{2}\left[\frac{\partial}{\partial t}(\alpha_{s_m}\rho_{s_m}\theta_{s_m}) + \nabla \cdot (\alpha_{s_m}\rho_{s_m}\vec{v}_{s_m}\theta_{s_m})\right] = (-P_{s_m}\bar{\bar{I}} + \bar{\bar{\tau}}_{s_m}) : \nabla \vec{v}_{s_m} + \nabla \cdot (k_{\theta_{s_m}}\nabla\theta_{s_m}) - \gamma_{\theta_{s_m}} + \varphi_{N\theta_{s_m}} \quad (19)$$

where $k_{\theta_{s_m}}$ represents the diffusion coefficient, while $\gamma_{\theta_{s_m}}$ denotes the collisional dissipation of energy and $\varphi_{I\theta_{s_m}}$ denotes the energy exchange between the nth gas or solid phase and the mth solid phase.

3.2. Cellulose pyrolysis model

The reaction mechanisms of the cellulose pyrolysis with and without potassium used in this work are developed by Ranzi et al. [32] and Trendewicz et al. [33], respectively. The latter is a modified version of the cellulose pyrolysis mechanism developed by Ranzi et al. [32], in order to include the effect of potassium on cellulose pyrolysis reactions. As shown in Table 2, four reactions were included in the pyrolysis mechanism: the depolymerization reaction of cellulose (R1), the fragmentation reaction of activated cellulose (R2), the depolymerization reaction of activated cellulose (R3), and the dehydration reaction of cellulose (R4-1 or R4-2).

All reactions were modeled using an Arrhenius expression:

$$k = A\exp[-E/RT] \quad (20)$$

The kinetic parameters for cellulose pyrolysis, as the functions of potassium concentration, are summarized in Tables 3 and 4.

As the fragmentation and depolymerization reactions of activated cellulose (CELLA) were inhibited and the depolymerization reaction of cellulose was catalyzed by potassium, the activation energies of reactions R2 and R3 increased with increasing potassium concentration. However, the activation energy of reaction R4-2 decreased. In this work, the temperature and concentration

Table 2
Pyrolysis reaction mechanism of cellulose with and without potassium [32,33].

Reaction No.	Reaction
R1	CELL → CELLA
R2	CELLA → 0.8HAA + 0.2GLYOX + 0.1 CH_3HCO + 0.25HMFU + 0.3C_3H_6O + 0.21CO_2 + 0.1H_2 + 0.4CH_2O + 0.16CO + 0.83H_2O + 0.02HCOOH + 0.61Char
R3	CELLA → LVG
R4-1[a]	CELL → 6Char + 5H_2O
R4-2[b]	CELL → 3Char + H_2O + 2CO + CO_2 + 4H_2

[a] The dehydration reaction of pure cellulose.
[b] The dehydration reaction of cellulose with potassium.

Table 3
Kinetic parameters of pure cellulose pyrolysis [33].

Reaction	Activation energy (kJ/mol)	Pre-exponent (1/s)
R1	188.4	4.0×10^{13}
R2	121.4	5.0×10^{8}
R3	41.9	1.8T
R4-1	129.8	4.0×10^{7}

Table 4
Kinetic parameters of cellulose pyrolysis with potassium [32,33].

Reaction	Activation energy (kJ/mol)	Pre-exponent (1/s)
R1	188.4	4.0×10^{13}
R2	$100.16x^{0.0168}$	3.78×10^{9}
R3	$118.99x^{0.056}$	2.61×10^{9}
R4-2	$124.52x^{0.03}$	2.00×10^{9}

x is mass fraction of potassium in cellulose.

gradients, and diffusion inside the particle were neglected as the biomass particles are very small.

3.3. Solution methodology

The fluidized bed is initially closed-packed up to 69.37 mm with the sand volume fraction of 0.618. The diameter of sand is 0.55 mm, and its initial temperature is same as the inlet fluidization gas temperature. All initial phase velocities are set to be zero.

The velocity inlet and mass flow inlet boundary conditions are used as the gas and biomass inlets, respectively. One atmospheric pressure boundary condition is used at the outlet of the fluidized bed. No-slip boundary and adiabatic walls are applied for all the walls. The k–ε turbulence model is used to model the effect of turbulence. The physical properties of particle phases are given in Table 5.

The simulations were conducted for a real reaction time of around 40–50 s, according to the solution convergence histories. The time-averaged yields of cellulose fast pyrolysis products were obtained from the last 10 s of the simulation. A time step size of 10^{-4} s and 50 iterations per time step were used.

4. Results and discussion

In this study, CFD simulations were conducted under five different potassium concentration and three different reactor temperature conditions to investigate the effects of potassium concentration and reactor temperature on the yield and the composition of cellulose fast pyrolysis products.

4.1. Hydrodynamics and fast pyrolysis in the fluidized bed reactor

Levoglucosan (LVG) is one of the main products of cellulose pyrolysis. The temporal-spatial evolutions of the gas phase flow velocity along with a LVG mass fraction of the pure cellulose pyrol-

Table 5
Physical properties of solid phases.

	Diameter (mm)	Density (kg/m^3)	Thermal conductivity W/(m K)	Specific heat capacity (kJ/kg K)
Sand	0.55	2650	0.35	835
Biomass	0.6	780	0.418	1500

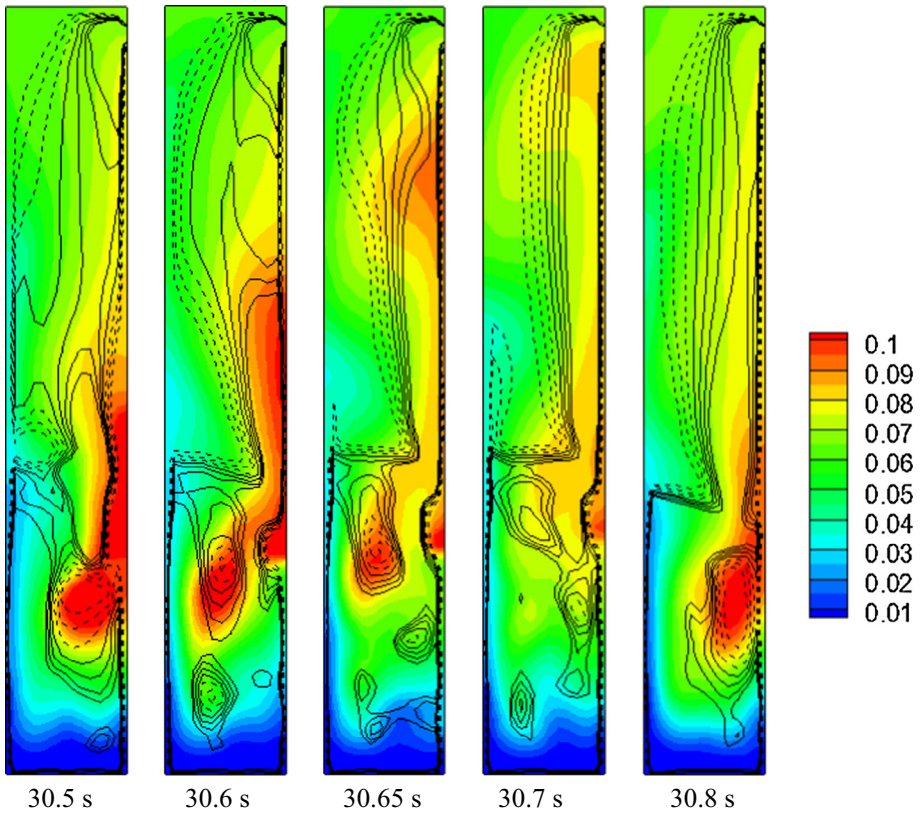

Fig. 2. Temporal-spatial evolutions of the LVG mass fraction and gas flow velocity (K = 0.0 wt.%, T_0 = 480 °C, solid lines: the gas velocity that higher than 0.744 m/s, dashed lines: the gas velocity that lower than 0.744 m/s).

ysis at T_0 = 480 °C are shown in Fig. 2. The contours and lines in the figure represent LVG mass fraction and gas phase flow velocity, respectively. The velocity that higher than 0.744 m/s is indicated using solid lines, and the dashed lines indicate the velocity that lower than 0.744 m/s. It can be seen that a high concentration region of the LVG occurs in the bed region at t = 30.5 s. This region is located within the low-velocity region of the fluidized bed, as LVG is released due to the devolatilization reaction and is not diluted rapidly in this region. However, LVG mass fraction near the outlet of the fluidized bed is low, resulting in a low yield of LVG. At the t = 30.6 s and 30.65 s, the high concentration LVG is observed at entrained and flowed downstream. At t = 30.7 s, as the high concentration LVG transports to the outlet of the fluidized bed, the LVG yield increases significantly (see Fig. 3(b)). At t = 30.8 s, the high concentration LVG near the outlet of the fluidized bed has been flowed out, while the new LVG formed in the fluidized bed has not been transported to the outlet, resulting in a dropped yield of the LVG (see Fig. 3(b)).

The yields of LVG and Hydroxyacetaldehyde (HAA) at the reactor outlet are shown in Fig. 3. LVG and HAA yields increase significantly in the initial stage (t < 5 s) of the biomass fast pyrolysis, then following by a drastic fluctuation in the yields. The significant fluctuation in the LVG yield is caused by the unstable flow in the fluidization zone that can affect the flow in the freeboard significantly, as the height of the fluidized bed is small in this work [22].

The ratio of LVG and HAA yields tends to be constant, as shown in Fig. 3(d), indicates that the fast pyrolysis process of cellulose in the fluidized bed reaches a steady state. The weak fluctuation of the yield ratio of LVG and HAA is likely to be dependent on non-uniform pyrolysis reaction temperature in the fluidized bed reactor.

4.2. Effect of potassium concentration on the product distribution of the cellulose fast pyrolysis

First, the simulation was performed to validate the present models. As shown in Table 6, the simulation results are in good agreement with the reported experimental data at 0.1% potassium concentration and temperature of T_0 = 500 °C [33]. Further, the effect of potassium concentration on the cellulose fast pyrolysis was studied at reactor temperature T_0 = 480 °C. As shown in the same Table, the enhancement of potassium concentration causes a significant reduction of the bio-oil and increase of the gas and char yields. The bio-oil yield decreases from 94.3% in pure cellulose case to 70.4% and 35.1% with 0.05% and 1.0% potassium concentration, respectively. The char yield increases from 2.5% in pure cellulose case to 16.6% and the gas yield increases from 3.3% in pure cellulose case to 48.3% at 1.0% potassium concentration. The effects of potassium concentration on the yields of the bio-oil, char and gas are consistent with the previous results in the literature [9–11,34].

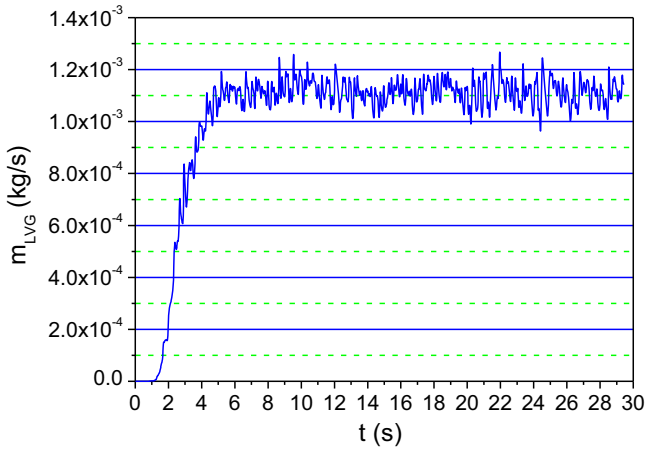

(a) The yield of LVG

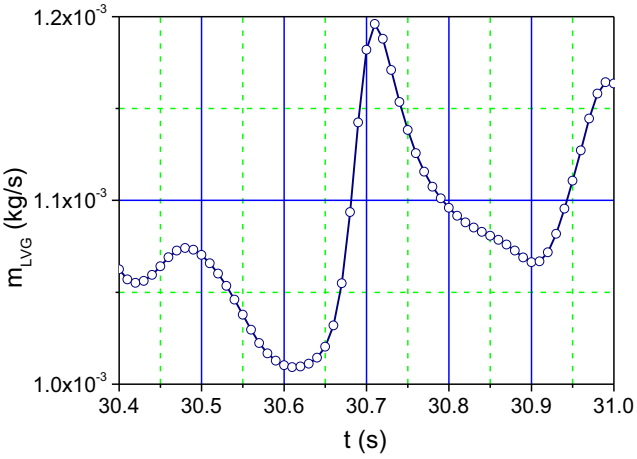

(b) The yield of LVG (t = 30.4 s – 31.0 s)

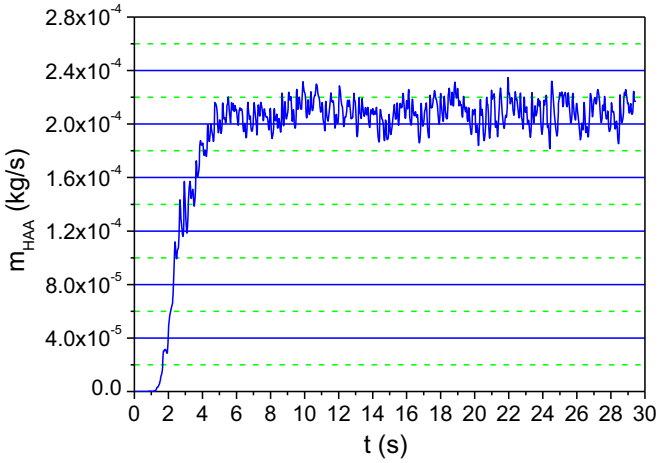

(c) The yield of HAA

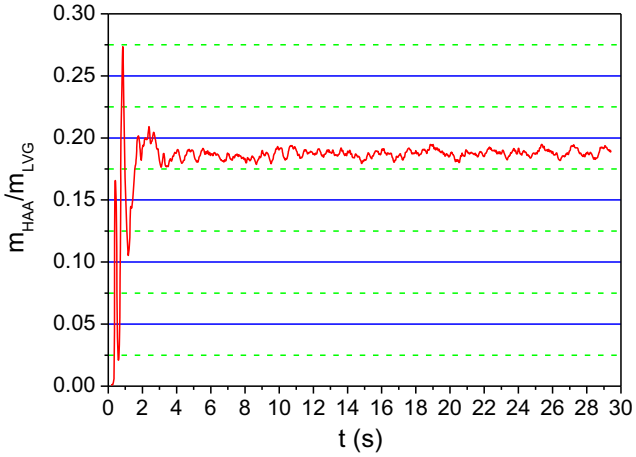

(d) Yield ratio of the HAA and LVG

Fig. 3. Evolutions of the yields of the LVG and HAA (K = 0.0 wt.%, T_0 = 480 °C).

Table 6
Effect of potassium concentration on the yields of biomass fast pyrolysis products.

Potassium (wt.%)	0.1 (T_0 = 500 °C) Simulation	0.1 (T_0 = 500 °C) Experiment [33]	0.0	0.05	0.1	0.5	1.0
			Simulation (T_0 = 480 °C)				
Bio-oil (wt.%)	66.4	68.6	94.3	70.4	61.8	41.5	35.1
Char (wt.%)	9.2	8.3	2.5	8.1	10.2	15.1	16.6
Gas (wt.%)	24.4	22.9	3.3	21.4	28.0	43.4	48.3

The main components of bio-oil found during cellulose pyrolysis are LVG, HAA, Hydroxymethylfurfural (HMFU), Acetone (C_3H_6O), H_2O, Formaldehyde (CH_2O), Glyoxal, Acetaldehyde (CH_3-HCO) and Formic acid (HCOOH). The composition of various components with respect to potassium concentration is shown in Fig. 4. As shown in Fig. 4(a), LVG mass fraction decreases from 63.8% of the bio-oil in pure cellulose case to 22.1% and 2.5% with 0.05% and 1.0% potassium concentration, respectively. The dramatic decrease of LVG mass fraction due to the inhibition of the depolymerization reaction of CELLA (R3) leads to decrease in LVG formation. The water mass fraction increases from 4.7% of the bio-oil in pure cellulose case to 29.7% at 1.0% potassium concentration. This behavior may be because water is formed through two reactions (R2 and R4) and the catalysis of the depolymerization reaction (R4-2) of cellulose results in the increased yields of water, as shown in Fig. 4(b).

As the potassium concentration increases from 0% to 0.1%, the mass fraction of HAA increases significantly, following by slight variations in the mass fraction of HAA when the potassium concentration further increases. The initial increase of the HAA mass fraction in bio-oil with potassium concentration caused by the inhibition of LVG formation (R3) occurs when competing with the HAA formation reaction (R2). The competition between R1 and R4-2 reactions results in the slight variation of the HAA mass fraction in bio-oil when potassium concentration increases from 0.1% to 1.0%. Moreover, the effects of potassium on the yields of other components in the bio-oil are similar to that of HAA.

The main components of produced non-condensable gas in the pyrolysis of cellulose are CO, CO_2 and H_2. As shown in Fig. 5(a), all of the yields of CO, CO_2 and H_2 increase significantly with increasing potassium concentration. It can be seen in Fig. 5(b) that the CO_2 mass fraction decreases from 66.4% to 42.1%, the CO mass fraction increases from 32.2% to 50.8%, and the H_2 mass fraction increases from 1.5% to 7.1%, respectively, as the potassium concentration increases from 0.0% to 1.0%. These compositions are formed via the R2 and R4 reactions. The CO_2 mass fraction of the gas produced

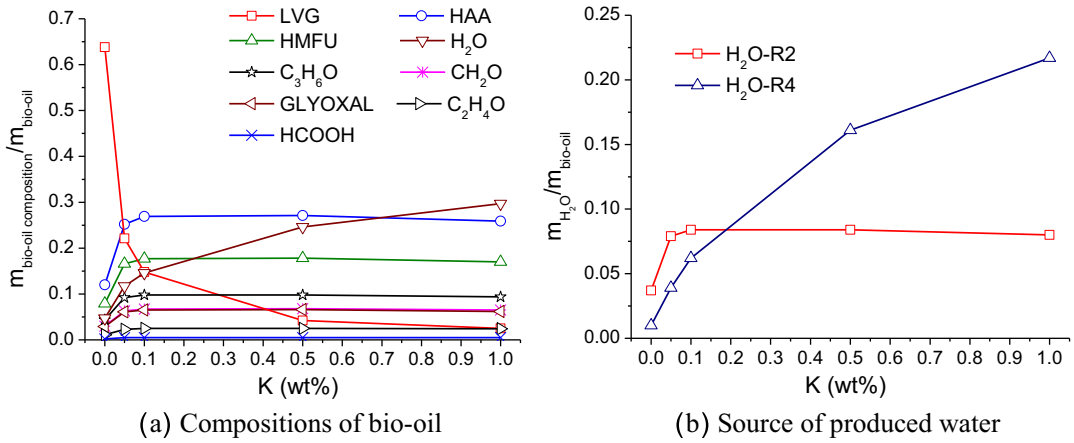

(a) Compositions of bio-oil (b) Source of produced water

Fig. 4. Effects of the potassium concentration on bio-oil compositions (T_0 = 480 °C).

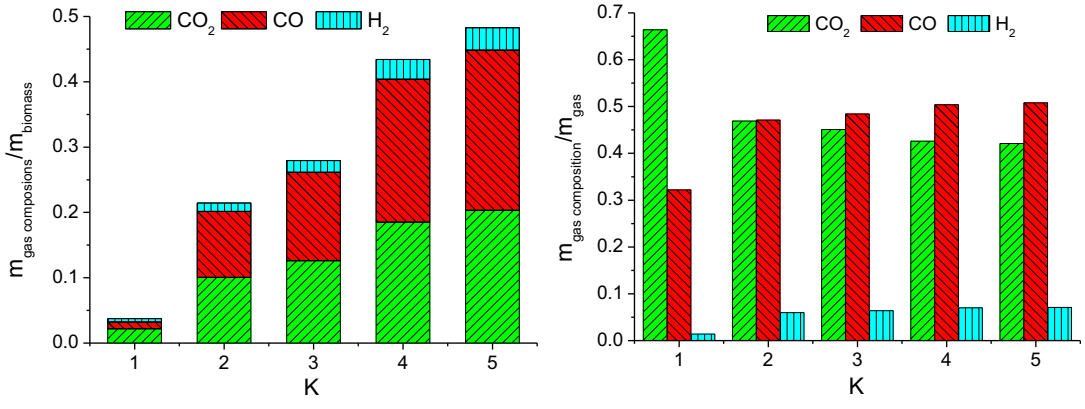

(a) The yields of gas (b) The compositions of gas

Fig. 5. Effects of the potassium concentration on gas compositions (T_0 = 480 °C, Potassium concentration: 1 – 0.0 wt.%, 2 – 0.05 wt.%, 3 – 0.1 wt.%, 4 – 0.5 wt.%, 5 – 1.0 wt.%).

in the R4 reaction is less than that produced in the R2 reaction. The decrease of CO_2 mass fraction and the increase of both CO and H_2 mass fraction with the increased potassium concentration are attributed to the inhibition of the R2 reaction and catalysis of the R4 reaction by the addition of potassium, which results in increases the gas yields significantly, as shown in Fig. 6.

4.3. Effect of reactor temperature on the cellulose fast pyrolysis

The temperature of the fluidized bed reactor is an important parameter that affects the thermochemical reactions. In the present study, the temperature of the fluidized bed reactor was varied by changing the temperature of the preheated fluidization gas. It can be seen in Table 7, as the reactor temperature increases from 430 °C to 515 °C, the yield of gas increases from 2.2% to 4.4% and the yield of char increases from 2.3% to 2.8% whereas the bio-oil yield decreases from 95.5% to 92.8% for the pure cellulose case. These behaviors may be because more tar is cracked to gas and char products at a higher temperature. This trend of product yields agrees with the literature for the pure cellulose [22,35]. However, the trend of the product yields for the cellulose with potassium is reversed when compared with the results of the pure cellulose case. As shown in Table 2, there is a significant difference between the dehydration reaction equations of the pure cellulose and cellulose with potassium (R4-1 and R4-2), i.e., the produced CO_2, CO and H_2 were incorporated in the equation R4-2. The increased reactor temperature promotes the endothermic R2 and R3 reactions, and the R4-2 reaction that forms gas is at a disadvantage in the competition with R2 and R3 reactions, so the gas yield decreases with increasing of the reactor temperature for the pyrolysis of cellulose with potassium.

In Table 8, as the reactor temperature increases from 430 °C to 515 °C, the mass fraction of LVG decreases and the mass fractions of other compositions in the bio-oil increase for the pyrolysis of the pure cellulose. The decrease of the LVG mass fraction is due to the competition of R2 and R3 reactions. For the fast pyrolysis of cellulose with 0.1% potassium, as the reactor temperature increases from 430 °C to 515 °C, the H_2O mass fraction decreases significantly, the mass fractions of LVG and all other bio-oil compositions increase. This is because the R2 and R3 reactions inhibited by potassium have a larger potential to be improved when the reactor temperature increases.

In Table 9, as the reactor temperature increases, the gas compositions of the pure cellulose pyrolysis are constant. This is because all gas compositions are from the same fragmentation reaction of activated cellulose (R2). For the fast pyrolysis of cellulose with

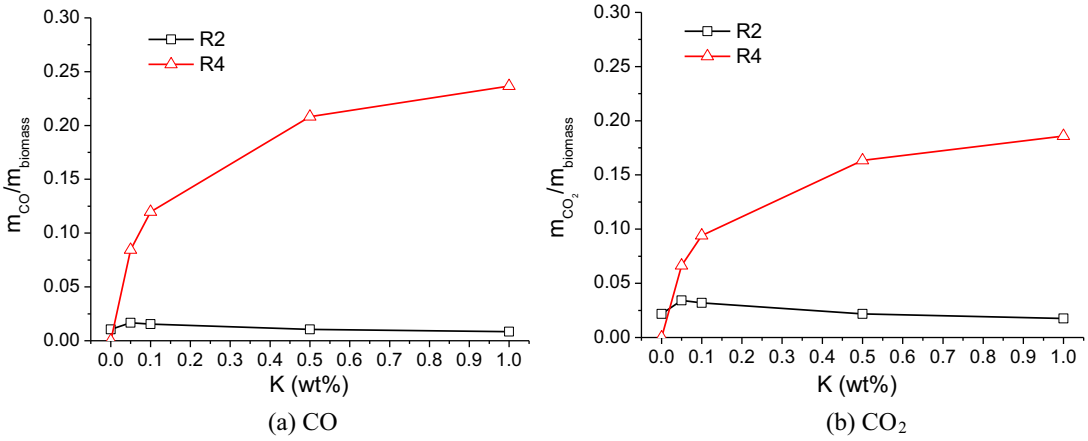

Fig. 6. Effects of the potassium concentration on sources of gas products (T_0 = 480 °C).

Table 7
Effect of reactor temperature on the pyrolysis products.

Potassium (wt.%)	0.0	0.0	0.0	0.1	0.1	0.1
T_0 (°C)	430	480	515	430	480	515
Oil (wt.%)	95.5	94.3	92.8	52.1	61.8	69.0
Char (wt.%)	2.3	2.5	2.8	12.6	10.2	8.5
Gas (wt.%)	2.2	3.3	4.4	35.4	28.0	22.5

Table 8
Effect of reactor temperature on the bio-oil compositions.

T_0 (°C)	430	480	515	430	480	515
Potassium (wt.%)	0.0	0.0	0.0	0.1	0.1	0.1
LVG	0.750	0.638	0.518	0.132	0.148	0.160
HAA	0.080	0.120	0.162	0.262	0.269	0.272
HMFU	0.053	0.079	0.106	0.172	0.177	0.179
C_3H_6O	0.029	0.044	0.059	0.095	0.098	0.099
CH_2O	0.020	0.030	0.040	0.065	0.067	0.068
GLYOXAL	0.019	0.029	0.039	0.063	0.065	0.066
C_2H_4O	0.007	0.011	0.015	0.024	0.025	0.025
HCOOH	0.002	0.002	0.003	0.005	0.005	0.005
H_2O	0.040	0.047	0.057	0.182	0.146	0.126

Table 9
Effect of reactor temperature on the gas compositions.

T_0 (°C)	430	480	515	430	480	515
Potassium (wt.%)	0.0	0.0	0.0	0.1	0.1	0.1
CO	0.322	0.322	0.322	0.496	0.484	0.471
CO_2	0.664	0.664	0.664	0.436	0.451	0.469
H_2	0.014	0.014	0.014	0.068	0.064	0.060

0.1% potassium, the CO_2 mass fraction increases from 43.6% to 46.9%, whereas the CO mass fractions decreases from 49.6% to 47.1%, and the H_2 mass fractions decreases from 6.8% to 6.0%, as the reactor temperature increases from 430 °C to 515 °C. The decrease of CO and H_2 mass fractions and the increase of CO_2 mass fraction are due to the fact that the elevated reactor temperature enhances the R2 and R3 reactions which form more CO_2 than R4 reaction.

5. Conclusions

In this study, the effect of potassium on the biomass fast pyrolysis in the fluidized bed reactor has been investigated using an Euler–Euler CFD model. The effects of potassium concentration and reactor temperature on the yield and component of pyrolysis products were analyzed. The simulation results indicate that the unstable flow in the fluidized bed results in the significant fluctuation in the product yield, and the weak fluctuation of the yield ratio between LVG and HAA is found. It is also observed that as the potassium concentration increases from 0% to 0.1%, the bio-oil yield decreases from 94.3% to 35.1% and the gas yield increases from 3.3% to 48.3%. Further, the addition of potassium leads to the significant change in the compositions of bio-oil and gas due to the inhibitions of decomposition reactions of activated cellulose and the catalysis of the depolymerization reactions of cellulose. For the effect of reactor temperature, the bio-oil yield decreases for the pure cellulose pyrolysis, while it has a reverse trend for the cellulose with potassium when the reactor temperature increases from 430 °C to 515 °C.

Acknowledgements

Authors gratefully acknowledge the financial support for this work by the UK Engineering and Physical Sciences Research Council (EPSRC) projects (EP/K036548/2; EP/J020184/2).

References

[1] Czernik S, Bridgwater AV. Overview of applications of biomass fast pyrolysis oil. Energy Fuels 2004;18:590–8.
[2] Guo MX, Song WP, Buhain J. Bioenergy and biofuels: history, status, and perspective. Renew Sustain Energy Rev 2015;42:712–25.
[3] Vamvuka D. Bio-oil, solid and gaseous biofuels from biomass pyrolysis processes – an overview. Int J Energy Res 2011;35:835–62.
[4] Bridgwater AV. Review of fast pyrolysis of biomass and product upgrading. Biomass Bioenergy 2012;38:68–94.
[5] Butler E, Devlin G, Meier D, McDonnell K. A review of recent laboratory research and commercial developments in fast pyrolysis and upgrading. Renew Sustain Energy Rev 2011;15:4171–86.
[6] Isahak WNRW, Hisham MWM, Yarmo MA, Yun Hin TY. A review on bio-oil production from biomass by using pyrolysis method. Renew Sustain Energy Rev 2012;16:5910–23.
[7] Nowakowski DJ, Bridgwater AV, Elliott DC, Meier D, de Wildd P. Lignin fast pyrolysis: results from an international collaboration. J Anal Appl Pyrol 2010;88:53–72.
[8] Xue Q, Dalluge D, Heindel TJ, Fox RO, Brown RC. Experimental validation and CFD modeling study of biomass fast pyrolysis in fluidized-bed reactors. Fuel 2012;97:757–69.
[9] Shimada N, Kawamoto H, Saka S. Different action of alkali/alkaline earth metal chlorides on cellulose pyrolysis. J Anal Appl Pyrol 2008;81:80–7.
[10] Patwardhan PR, Satrio JA, Brown RC, Shanks BH. Influence of inorganic salts on the primary pyrolysis products of cellulose. Bioresour Technol 2010;101:4646–55.
[11] Rutkowski P. Pyrolysis of cellulose, xylan and lignin with the K_2CO_3 and $ZnCl_2$ addition for bio-oil production. Fuel Process Technol 2011;92:517–22.
[12] Hu S, Jiang L, Wang Y, Su S, Sun L, Xu B, et al. Effects of inherent alkali and alkaline earth metallic species on biomass pyrolysis at different temperatures. Bioresour Technol 2015;192:23–30.
[13] Di Blasi C, Galgano A, Branca C. Influences of the chemical state of alkaline compounds and the nature of alkali metal on wood pyrolysis. Ind Eng Chem Res 2009;48:3359–69.
[14] Jensen A, Dam-Johansen K, Wojtowicz MA, Serio MA. TG-FTIR study of the influence of potassium chloride on wheat straw pyrolysis. Energy Fuels 1998;12:929–38.
[15] Mourant D, Wang ZH, He M, Wang XS, Garcia-Perez M, Ling KC, et al. Mallee wood fast pyrolysis: effects of alkali and alkaline earth metallic species on the yield and composition of bio-oil. Fuel 2011;90:2915–22.
[16] Xue Q, Heindel TJ, Fox RO. A CFD model for biomass fast pyrolysis in fluidized-bed reactors. Chem Eng Sci 2011;66:2440–52.
[17] Boateng AA, Mtui PL. CFD modeling of space-time evolution of fast pyrolysis products in a bench-scale fluidized-bed reactor. Appl Therm Eng 2012;33–34:190–8.
[18] Mellin P, Zhang QL, Kantarelis E, Yang WH. An Eulre-Euler approach to modeling biomass fast pyrolysis in fluidized-bed reactors – focusing on the gas phase. Appl Therm Eng 2013;58:344–53.
[19] Xiong QG, Kong SC, Passalacqua A. Development of a generalized numerical framework for simulating biomass fast pyrolysis in fluidized-bed reactors. Chem Eng Sci 2013;99:305–13.
[20] Sharma A, Wang SB, Pareek V, Yang H, Zhang DK. CFD modeling of mixing/segregation behavior of biomass and biochar particles in a bubbling fluidized bed. Chem Eng Sci 2014;106:264–74.
[21] Mellin P, Zhang QL, Kantarelis E, Yang WH. Computational fluid dynamics modeling of biomass fast pyrolysis in a fluidized bed reactor, using a comprehensive chemistry scheme. Fuel 2014;117:704–15.
[22] Sharma A, Wang SB, Pareek V, Yang H, Zhang DK. Multi-fluid reactive modeling of fluidized bed pyrolysis process. Chem Eng Sci 2015;123:311–21.
[23] Ranganathan P, Gu S. Computational fluid dynamics modeling of biomass fast pyrolysis in flusized bed reactors, focusing different kinetic schemes. Bioresour Technol 2016;213:333–41.
[24] Papadikis K, Gu S, Bridgwater AV, Gerhauser H. Application of CFD to model fast pyrolysis of biomass. Fuel Process Technol 2009;90:504–12.
[25] Bruchmuüller J, van Wachem BGM, Gu S, Luo KH, Brown RC. Modeling the thermochemical degradation of biomass inside a fast pyrolysis fluidized bed reactor. AICHE J 2012;58:3030–42.
[26] Bruchmuüller J, Luo KH, van Wachem BGM. Tar formation variations during fluidised bed pyrolytic biomass conversion. Proc Combust Inst 2013;34:2373–81.
[27] Papadikis K, Gu S, Bridgwater AV. CFD modelling of the fast pyrolysis of biomass in fluidized bed reactors. Part B Heat, momentum and mass transport in bubbling fluidized beds. Chem Eng Sci 2009;64:1036–45.
[28] Patel M. Pyrolysis and gasification of biomass and acid hydrolysis residues PhD Thesis. UK: Aston University; 2013.
[29] ANSYS FLUENT 15.0, Theory Guide; ANSYS Inc.; 2012.
[30] Gidaspow D, Bezburuah R, Ding J. Hydrodynamics of circulating fluidized beds: kinetic theory approach. In: Fluidization VII, Proceedings of the 7th engineering foundation conference on fluidization. p. 75–82.
[31] Gunn DJ. Transfer of heat or mass to particles in fixed and fluidized beds. Int J Heat Mass Transfer 1978;21:467–76.
[32] Ranzi E, Corbetta M, Manenti F, Pierucci S. Kinetic modeling of the thermal degradation and combustion of biomass. Chem Eng Sci 2014;110:2–12.
[33] Trendewicz A, Evans R, Dutta A, Sykes R, Carpenter D, Braun R. Evaluating the effect of potassium on cellulose pyrolysis reaction kinetics. Biomass Bioenergy 2015;74:15–25.
[34] Hwang H, Oh S, Cho TS, Choi IG, Choi JW. Fast pyrolysis of potassium impregnated poplar wood and characterization of its influence on the formation as well as properties of pyrolytic products. Bioresour Technol 2013;150:359–66.
[35] Xiong QG, Aramideh S, Kong SC. Modeling effects of operating conditions on biomass fast pyrolysis in bubbling fluidized bed reactors. Energy Fuels 2013;27:5948–56.